Free Vibration Analysis of Aboveground LNG-Storage Tanks by the Finite Element Method

Jin-Rae Cho*, Jin-Kyu Lee, Jeong-Mok Song
School of Mechanical Engineering, Pusan National University
Suk-Ho Park, Joong-Nam Lee
Samsung Heavy Industries Co., Ltd.

Recently, in proportion to the increase of earthquake occurrence-frequency and its strength in the countries within the circum-pan Pacific earthquake belt, a concept of earthquake-proof design for huge structures containing liquid has been growing up. This study deals with the refinement of classical numerical approaches for the free vibration analysis of separated structure and liquid motions. According to the liquid-structure interaction, LNG-storage tanks exhibit two distinguished eigenmodes, the sloshing mode and the bulging mode. For the sloshing -mode analysis, we refine the classical rigid-tank model by reflecting the container flexibility. While, for the bulging-mode analysis, we refine the classical uncoupled structural vibration system by taking the liquid free-surface fluctuation into consideration. We first construct the refined dynamic models for both problems, and present the refined numerical procedures. Furthermore, in order for the efficient treatment of large-scale matrices, we employ the Lanczos iteration scheme and the frontal-solver for our test FEM program. With the developed program we carry out numerical experiments illustrating the theoretical results.

Key Words : LNG-Storage Tank, Fluid-Structure Interaction, Finite Element Analysis, Sloshing Mode, Bulging Mode, Structure Deformation, LNG Free-Surface Fluctuation.

1. Introduction

As an uncontaminated fuel, the need of LNG (Liquefied Natural Gas) has greatly grown up, and accordingly its storage tanks are on the trend of a large size. However, unexpected structural failure of such huge structures by earthquakes may result in not only severe environmental contamination but also tremendous loss of human and financial resources. In the countries within the circum-pan Pacific earthquake belt, an earthquake-proof structural design is a matter of primary concern. In order for such an earthquake-proof design, accurate eigenmode analysis and seismic analysis with reliable earthquake record are of a great importance.

In the liquid-structure interaction system composed of LNG container, relatively dense LNG and other subsidiary components, the eigen-behavior is characterized by the sloshing and bulging modes. The former is called a displacement-type eigenmode characterizing by the LNG free-surface motion, while the latter is called an acceleration-type eigenmode dominated by the container deformation. According to a weak dynamic coupling between two modes, analysts used to separate the whole integrated dynamic system into two uncoupled regions, a container for the bulging mode and a liquid for the sloshing mode.

Best to our memory, theoretical and experimental studies on the eigen behavior of liquid-storage tanks were done by Haroun (1983, 1985 and

* Corresponding Author,
E-mail : jrcho@hyowon.pusan.ac.kr
TEL : +82-51-510-2467 ; **FAX** : +82-51-514-7640
School of Mechanical Engineering, Pusan national University, Jangjeon-dong, Kumjung Pusan 609-735, Korea. (Manuscript **Received** October 19, 1999; **Revised** march 15, 2000)

1996) and Ohayon et al. (1995), and the finite element analysis of eigenmodes of such tanks was carried out by Okada et al. (1975), Tedesco et al. (1989) and Khai (1993). In particular, Okada et al. considered the entire dynamic system consisting of LNG and shell-like container as a coupled integration system for the finite element analysis. As for the computation of equivalent mass added to the structure, Gupta (1976), Rajasankar et al. (1993) and Zienkiewicz et al. (1991) introduced their numerical techniques. A recent study on the added mass of viscous fluid-structure interaction problems by Conca et al. (1997) is also worth to mention.

These studies can be largely classified into two, some for the coupled entire liquid-structure system and others for the uncoupled structure and liquid. In the former, the container flexibility as well as the liquid free-surface fluctuation are inherently reflected. But, in the latter, both interference effects have been neglected, owing to the numerical difficulty and complexity.

This paper is concerned with the refinement of the latter classical approaches. For this goal, we refine the classical rigid-tank model, for the liquid sloshing motion, by including the container flexibility. As well as, we take the liquid free-surface fluctuation into the added-mass computation, for the structure bulging motion. Through the numerical experiments with a model LNG-storage tank, we compute eigen frequencies and modes by the refined procedures and carry out the comparison of the refined methods with classical approaches.

2. LNG-Storage Tanks and Dynamic Modeling

2.1 LNG-storage tanks

Figure 1 shows a general aboveground LNG-storage tank. A shell-like thin structure manufactured by Ni-Cr steel is supported on the ferrite layer mounted on the concrete base. In order to avoid its vertical and horizontal rigid movement, it is jointed with pre-tensioned anchor bolts positioned uniformly in the circumferential direction. A shell-like container consists of four

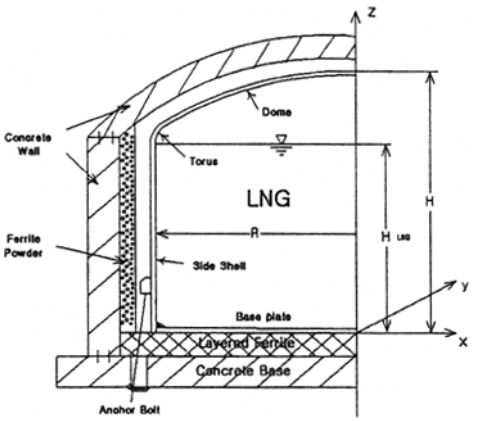

Fig. 1 A structure of above-ground LNG-storage tank

parts, the base plate, the side shell, the upper dome and the torus joining the side shell and the upper dome. The relative thickness to the tank radius of LNG-storage tanks in most engineering applications is of 10^{-3} order, so the container is ultra-thin structure.

An exterior concrete wall is for the sake of protecting the container from various kinds of external attacks. The bottom ferrite layer inserted between the base plate and the concrete base plays a role of shock absorbing and insulation. The other ferrite powder filled up between the exterior concrete wall and the side shell is just for insulation.

Here, we exclude the exterior concrete wall and the side ferrite powder from the eigenmode analysis because the dynamic-interaction effect on the LNG-storage tank by those components is of negligible amount. In addition, since we are interested in the horizontal eigen-characteristics, we simplify the bottom ferrite layer as a rigid layer such that the base plate of shell-like container is constrained such that no relative dynamic motion with respect to the concrete base is allowed.

2.2 Dynamic model for the bulging mode and FE approximation

As mentioned before, in the bulging mode the deformation of container is dominated while the free-surface fluctuation of interior LNG is feeble. Based on this weak coupling between the two modes (Haroun 1983, Haroun et al. 1985), it has

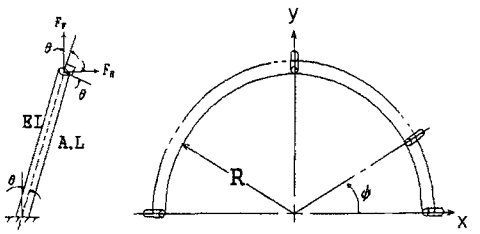

Fig. 2 Uniformaly arranged anchor bolts (91EA × 2°) and the cantilever beam model

been traditional to split a liquid-structure interaction system into two equivalent uncoupled dynamic systems for separate container and liquid regions.

In order to construct a reliable uncoupled dynamic model for the bulging mode under consideration, computation of accurate equivalent added-mass of LNG and equivalent spring constants of anchor bolts is an important step. The classical numerical technique to compute added-mass corresponding to the hydrodynamic effect is now well established. The reader may refer to Rajasankar et al. (1993) and Zienkiewicz and Taylor (1991). Here, we refine it by including the LNG free-surface fluctuation.

Referring to Fig. 2, we simplify the anchor bolts as a cantilever beam of circular section, to which we apply the unit load method to obtain the component-wise equivalent spring constants k_n^x, k_n^y and k_n^z of the n-th anchor bolt given by

$$\begin{aligned} 1/k_n^x &= \frac{L}{EI}(\sin^2\psi_n + \cos^2\psi_n \cdot \sin^2\theta) \\ &\quad + \frac{L}{EA}\cos^2\psi_n \cdot \cos^2\theta \\ 1/k_n^y &= \frac{L}{EI}(\cos^2\psi_n + \sin^2\psi_n \cdot \sin^2\theta) \\ &\quad + \frac{L}{EA}\sin^2\psi_n \cdot \cos^2\theta \\ 1/k_n^z &= \frac{L\sin^2\theta}{EI} + \frac{L\cos^2\theta}{EA} \end{aligned} \tag{1}$$

Denoting the domain of shell-like container by $\Omega \in \Re^3$, we write the dynamic equilibrium equations together with the essential and natural boundary conditions (i, j, k=x, y, z and k; no sum):

$$\left.\begin{aligned} &\sigma_{ij}(\mathbf{u})_{,j} - \rho\frac{d^2u_i}{dt^2} = 0, && \text{in } \Omega \\ &u_i = 0, && \text{on } \partial\Omega_D \\ &-\sigma_{ij}n_in_j = p, && \text{on } \partial\Omega_I \\ &-\sigma_{ij}n_j = k_s^k(\psi_n)u_k, && \text{on } \partial\Omega_N^n \end{aligned}\right\} \tag{2}$$

where ρ denotes the density of the structure. Furthermore, σ_{ij} and $\mathbf{n}$ indicate Cauchy stress-tensor components and the outward unit vector normal to the structure, respectively. The hydrodynamic pressure $p \in L^2(\partial\Omega_I)$ on the liquid-structure interface $\partial\Omega_I$ by interior LNG is transformed into the equivalent mass added to the structure, as described in Appendix I. The other natural boundary condition is the dynamic spring forces on $\bigcup_n \partial\Omega_N^n$ by anchor bolts.

In order to construct the corresponding variational statement of the eigenvalue problem (2), we first define the triple vector-valued function space $V(\Omega)$ of admissible displacement fields

$$V(\Omega) = \{v \in [H^1(\Omega)]^3 | v = 0 \text{ on } \partial\Omega_D\} \tag{3}$$

Treating the dynamic spring forces by anchor bolts as point loads, we obtain the variational form of the problem (2): Find $\{\omega \in \Re, \mathbf{u}(\mathbf{x}) \in V(\Omega)\}$ such that $\forall \mathbf{v} \in V(\Omega)$,

$$\begin{aligned} &\int_\Omega \varepsilon_{ij}(\mathbf{v})\,\sigma_{ij}(\mathbf{u})\,d\Omega + \sum_n [v_i(k^i u_i)]_n \\ &= \omega^2 \int_\Omega \rho v_i u_i d\Omega - \int_{\partial\Omega_I} p\mathbf{v}\cdot\mathbf{n}\,ds \end{aligned} \tag{4}$$

where $\{\omega, \mathbf{n}(x)\}$ denotes eigen sets corresponding to the bulging mode.

Using three-dimensional isoparametric 20-node cubic and 15-node tetrahedron elements, we approximate the dynamic displacement fields:

$$\mathbf{u}^h = \mathbf{N}\bar{\mathbf{u}} \tag{5}$$

by denoting $\mathbf{N}$ and $\bar{\mathbf{u}}$ as a matrix containing corresponding finite-element basis functions $\{\varphi_k(\mathbf{x})\}_{k=1}^N$ and the nodal vector, respectively. Corresponding strain and stress tensors are written as

$$\varepsilon(\mathbf{u}^h) = \mathbf{DN}\bar{\mathbf{u}} = \mathbf{B}\bar{\mathbf{u}} \tag{6}$$

$$\sigma(\mathbf{u}^h) = \mathbf{EB}\bar{\mathbf{u}} \tag{7}$$

with a (3x6) divergence-like operator $\mathbf{D}$ defining Cauchy strain tensor and the (6x6) three-dimensional linear-elastic material matrix $\mathbf{E}$ containing Lame constants μ and λ.

Substituting the finite element approximations into the variational problem (4), we have the general numerical eigenvalue problem:

$$[\mathbf{K}-\omega^2\mathbf{M}_b]\bar{\mathbf{u}}=0 \tag{8}$$

Here, two matrices are defined respectively as

$$\mathbf{K}=\int_\Omega \mathbf{B}^T\mathbf{E}\mathbf{B}\ d\Omega+\sum_n(\mathbf{N}^T\mathbf{k}_n\mathbf{N})_n \tag{9}$$

$$\mathbf{M}_b=\int_\Omega \rho\mathbf{N}^T\mathbf{N}\ d\Omega+\rho_L(\mathbf{H}\mathbf{R})^T\mathbf{S}_I^{-1}(\mathbf{H}\mathbf{R}) \tag{10}$$

where $\mathbf{k}_n$ denotes diag(k_n^x, k_n^y, k_n^z) and ρ_L the density of LNG. The RHS term in Eq. (10) is the equivalent mass matrix of LNG added to the structure. Its detailed numerical derivation is given in Appendix A.1.

2.3 Dynamic model for the sloshing mode and FE approximation

On the contrary to the bulging mode, in the sloshing mode the free-surface fluctuation of LNG prevails while the structure-deformation is of negligible amount. And hence, it has been conventional to assume it as a rigid-tank sloshing (Haroun 1983). For the assessment on this classical model, Okada et al. (1975) and Khai (1993) compared the eigen frequencies obtained by the rigid-tank sloshing model and the coupled integration system. According to their results, it has been found that the classical model is acceptable for most engineering applications within the relative modeling error less than 1%. Differing from them, we in this study directly refine the classical model in order to account for the container deformation and intend to examine the container-deformation effect on the LNG sloshing mode.

Since our study aims at the horizontal eigen-behavior, we consider a half of LNG region, as depicted in Fig. 3, where boundary definition together with corresponding boundary conditions in terms of the velocity vectors, $\mathbf{v}$ of LNG and $\mathbf{v}_s$ of the structure, and the hydrodynamic pressure are described. For the fluid motion, we assume that the fluctuation of LNG is incompressible, inviscid and irrotational (i. e. curl-free: $\nabla\times\mathbf{v}=0$). Then, for the free-surface vibration of ideal flow, there exists a potential function $\varphi(\mathbf{x};\ t)$

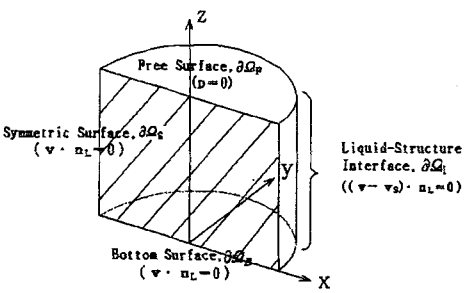

Fig. 3 Boundary definition of the half of LNG region

satisfying

$$\varphi:\ \mathbf{v}(\mathbf{x};\ t)=\nabla\varphi \tag{11}$$

The behavior of free-surface vibration of ideal flow is governed by Laplace equation from the continuity equation

$$\nabla\cdot\mathbf{v}=\nabla^2\varphi=0,\ \text{in}\ \Omega_L \tag{12}$$

and the corresponding boundary conditions (Currie 1974)

$$\left.\begin{aligned}&\nabla\varphi\cdot\mathbf{n}_L=-\frac{\partial^2\varphi}{g\cdot\partial t^2},\ \text{on}\ \partial\Omega_F\\&\nabla\varphi\cdot\mathbf{n}_L=\mathbf{v}_S\cdot\mathbf{n}_L,\ \text{on}\ \partial\Omega_I\\&\nabla\varphi\cdot\mathbf{n}_L=0,\ \text{on}\ \partial\Omega_B\ \text{and}\ \partial\Omega_S\end{aligned}\right\} \tag{13}$$

Here, $\Omega_L\in\Re^3$ and $\mathbf{n}_L$ are the LNG domain and the outward unit vector normal to its boundary (i. e., $\mathbf{n}_L\cdot\mathbf{n}=-1$) respectively.

Here, for our study, we record the fundamental relations associated with the simple harmonic motion. First, taking the spatial integration to the Euler equation $(\nabla p+\rho_L\dot{\mathbf{v}}=\mathbf{0})$, we have

$$p(\mathbf{x};\ t)=-\rho_L\partial\varphi(\mathbf{x};\ t)/\partial t,\ \text{in}\ \Omega_L \tag{14}$$

Then, we can establish the alternative Helmholtz equation and boundary conditions in terms of the hydrodynamic pressure to Eqs. (12) and (13). Second, using the fact of ($\dot{\eta}=v_z=\nabla\varphi\cdot\mathbf{n}_L$, $\eta\sim$the sloshing height of the LNG free-surface) and the corresponding boundary condition in Eq. (13), we have the relation given by

$$\eta=-\frac{1}{g}\frac{\partial\varphi}{\partial t},\ \text{on}\ \partial\Omega_F \tag{15}$$

Defining the space of admissible potential functions as $V(\Omega_L)=H^1(\Omega_L)$ and applying the boundary conditions specified in Eq. (13), we

obtain the variational form of the eigen-behavior of the free-surface vibration problem (12): Find $\{\omega \in \Re,\ \varphi(\mathbf{x}) \in V(\Omega_L)\}$ such that

$$\int_{\Omega_L} \nabla\chi \cdot \nabla\varphi \, d\Omega - \int_{\partial\Omega_I} \chi(\mathbf{v}_s \cdot \mathbf{n}_L) ds = \frac{\omega^2}{g} \int_{\partial\Omega_F} \chi\varphi ds, \ \forall \chi \in V(\Omega_L) \tag{16}$$

The above formulation involves the liquid-structure coupling, the second term in the LHS, but which vanishes when we assume the rigid-tank sloshing.

With the same finite elements used for the bulging mode, we construct the finite element approximations of potential functions and normal velocities $\dot{u}_n$ of the structure as follows

$$\varphi^h = \Phi\bar{\varphi},\ \dot{u}_n^h = -(\mathbf{u}_s \cdot \mathbf{n}_L)^h = \Phi\tilde{\mathbf{u}}_n \tag{17}$$

where Φ is a matrix containing finite-element basis functions.

Splitting the global finite-element nodes into those on the free-surface (denoted by F) and the rest (denoted by R) and enlarging $\mathbf{H}$ matrix such that the nodal vector $\tilde{\mathbf{u}}_n$ on $\partial\Omega_I$ can be extended to whole nodes in Ω_L, we have

$$\left\{\begin{bmatrix} \mathbf{K}_{FF} & \mathbf{K}_{FR} \\ \mathbf{K}_{RF} & \mathbf{K}_{RR} \end{bmatrix} - \omega^2 \begin{bmatrix} \mathbf{M} & \mathbf{0} \\ \mathbf{0} & \mathbf{0} \end{bmatrix}\right\} \begin{Bmatrix} \bar{\varphi}_F \\ \bar{\varphi}_R \end{Bmatrix} = -\begin{bmatrix} \mathbf{H}_{FF} & \mathbf{H}_{FR} \\ \mathbf{H}_{RF} & \mathbf{H}_{RR} \end{bmatrix} \begin{Bmatrix} \tilde{\mathbf{u}}_n^F \\ \tilde{\mathbf{u}}_n^R \end{Bmatrix} \tag{18}$$

where each matrix is defined as

$$\mathbf{M} = \frac{1}{g}\int_{\partial\Omega_F} \Phi^T\Phi \, ds,\ \mathbf{K} = \int_{\Omega_L} \nabla\Phi \cdot \nabla\Phi \, d\Omega,\ \mathbf{H} = \int_{\partial\Omega_I} \Phi^T\Phi \, ds \tag{19}$$

The detailed numerical derivation on correlating the normal velocity with the potential function is described in Appendix A.2. Along the procedure in Appendix A.2 for transforming the dynamic effect of the container deformation into the equivalent mass matrix for the bulging mode, we finally arrive at

$$\left\{\begin{bmatrix} \mathbf{K}_{FF} & \mathbf{K}_{FR} \\ \mathbf{K}_{RF} & \mathbf{K}_{RR} \end{bmatrix} - \omega^2 \begin{bmatrix} \mathbf{M}+\hat{\mathbf{M}}_{FF} & \hat{\mathbf{M}}_{FR} \\ \hat{\mathbf{M}}_{RR} & \hat{\mathbf{M}}_{RR} \end{bmatrix}\right\} \begin{Bmatrix} \bar{\varphi}_F \\ \bar{\varphi}_R \end{Bmatrix} = \begin{Bmatrix} \mathbf{0} \\ \mathbf{0} \end{Bmatrix} \tag{20}$$

We note that the equivalent mass is also frequency dependent, as described in Eq. (A15).

3. Iterative Numerical Algorithm

For relatively small-size matrices of $[\mathbf{K}]$ and $[\mathbf{M}]$, one can obtain eigen sets $\{\omega, \bar{\mathbf{u}}\}$ by direct methods such as the inverse or the forward iteration techniques. But, in most engineering problems, these two matrices are large-scale so that it may beyond the limit of computation capability to handle whole array elements.

Fortunately, in many cases of structural vibration analysis, several lowest eigen sets are enough for the acceptable dynamic behavior of the problem under consideration, and hence rapid and efficient numerical algorithms such as the Lanczos iteration method, the subspace method and so on are widely used. To implement our theoretical results, we develop a test FEM program equipped with the iterative numerical algorithm utilizing the Lanczos method, the frontal solver and the mass-lumping technique.

As is well known, the Lanczos iteration method transforms the full $(N \times N)$ eigen-matrix system $(\mathbf{Ku} = \omega^2\mathbf{Mu})$ to the truncated $(n \times n)$ system $(n < N)$

$$\mathbf{T}_u\tilde{\mathbf{u}} = \frac{1}{\omega^2}\tilde{\mathbf{u}} \tag{21}$$

where, the truncation operator $\mathbf{T}_n$ is constructed with $\{\alpha_i, \beta_i\}$ that are iteratively computed, as shown in the flowchart. The truncated eigen-system (21) is of relatively small size so that one can easily obtain corresponding eigen-sets with usual direct methods. Since the reader is familiar with such numerical techniques, we leave the detailed description to the reference (Bathe 1996).

Referring to the flowchart, in order to compute $\bar{\mathbf{x}}_i$ and $\{\alpha_i, \beta_i\}$ using the Lanczos method, we still need full stiffness and mass matrices. In order to avoid the need of large-scale storage, we utilize the frontal solver and the mass-lumping technique, as depicted in Fig. 4. The mass matrix becomes a diagonal matrix by means of the mass-lumping technique, and hence its global storage is reduced to N. Then, the computation of

$$\mathbf{K}\bar{\mathbf{x}}_i = \mathrm{diag}(\mathbf{M})\,\mathbf{x}_i \tag{22}$$

at each Lanczos iteration can be carried out by

Table 1 Numerical data for the simulation

Material data			Geometry data (cm)	
Ni-Cr Steel	Density (kgf·sec²/cm⁴), ρ	2.67 ($\times 10^{-5}$)	Container radius, R	2500
	Young's modulus (kgf/cm²), E	7.0 ($\times 10^{5}$)	Container height, H	3975.5
			Side-shell thickness	5.15-1.65
	Poisson's ratio, ν	0.3	Dome/torus thickness	1.65
LNG	Density (kgf·sec²/cm⁴), ρ_L	4.6 ($\times 10^{-7}$)	LNG height, H_{LNG}	3000
			Anchor bolt diameter, d	3.6
			Anchor bolt length, L	300
			Angle, θ	15°

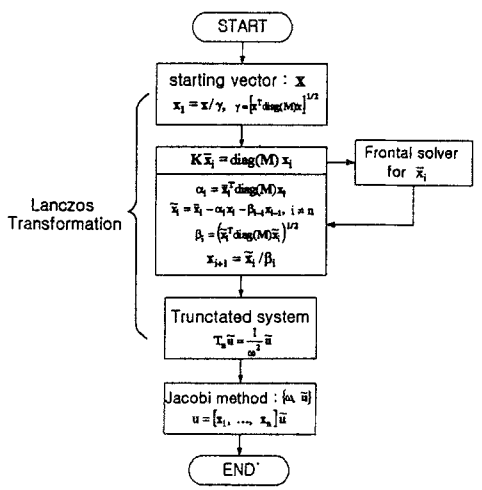

Fig. 4 Flowchart for iterative numerical algorithm employed in the test FEM program

the usual frontal solver because the RHS in Eq. (22) is simplified to an element-wise load vector.

4. Numerical Results

For the numerical simulation of eigen-characteristics of LNG storage tanks, we develop a test FEM program equipped with the pre-mentioned iterative numerical algorithm. In order to visualize the numerical results and the geometry of LNG-storage tanks, we utilize the pre- and post-processing modules of the commercial ANSYS software.

For the numerical experiments, we consider a closed-type aboveground LNG-storage tank capable of storing 6000k*l* LNG. Referring to Fig. 1, the interior LNG is filled up to the height of H_{LNG}, and the container and the anchor bolts are manufactured by Ni-Cr steel. The side-shell thickness varies continuously along the z-axis ranging from 5.15cm at the bottom to 1.65cm at the other end. Table 1 contains the material properties of Ni-Cr steel and LNG and representative geometry data of the model LNG-storage tank.

Referring to Figs. 8 and 9, we generate finite element meshes for the container and the interior LNG using three-dimensional quadratic elements. We made the same finite-element partition on the common liquid-structure interfaces so that the numerical treatment for converting the hydrodynamic pressure to the added-mass for the bulging mode and reflecting the shell deformation in the sloshing mode is easily carried out.

4.1 Results of the bulging mode

According to the numerical procedure described in this paper, we calculate the added-mass matrices. However, since it requires natural frequencies *a priori*, as described in Appendix A.1, we apply the sort of predictor and corrector method. In other words, we first simulate the bulging mode without the free-surface fluctuation, in which the added-mass is frequency-independent, and next we obtain the added-mass matrix and natural frequency corresponding to each of the pre-computed natural frequencies for the case without free-surface fluctuation.

Figure 5 shows the variations of total added-

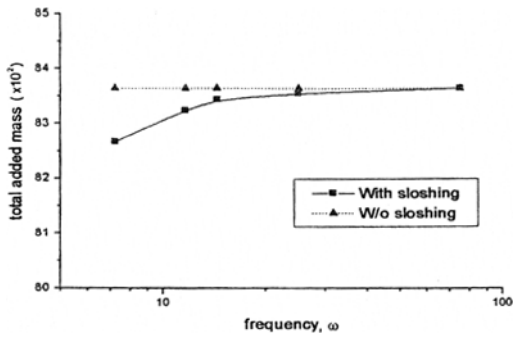

Fig. 5 Variations of the calculated total added-mass to the natural frequency

mass with respect to the natural frequency. When the free-surface fluctuation is neglected, 61.7% of the total LNG mass is added to the structure. On the other hand, the total added-mass when the free-surface sloshing is included varies along the natural frequency, while it approaches that of the case without the free-surface fluctuation. For a reference, it drops to 60.9% of the total LNG mass at the lowest natural frequency, and which is relatively 1.3% smaller than the case without the free-surface fluctuation.

Next, we examine the distributions of nodal added masses on the side-shell interface. According to our assumption of ideal fluid-flow, the added-mass component m_z identically vanishes on that surface. For the spatial distribution, we diagonalize the added-mass matrix and assume each diagonal value as the lumped mass at the corresponding finite-element node. Since we uniformly partitioned the liquid-structure interface along the axial and the circumferential directions, respectively, this assignment makes sense.

Figure 6 presents respectively the vertical and the sectional distributions of nodal added-mass components, where the case with sloshing corresponds to the distributions obtained by including the free-surface fluctuation with the lowest natural frequency. From the vertical distributions shown in Fig. 6(a), we see that the case with the free-surface sloshing has non-zero added-mass at the free surface. This implies that the corresponding hydrodynamic pressure at that surface is not zero, as given in Eqs. (14) and (15). On the other hand, the x-component exhibits cosine-type sec-

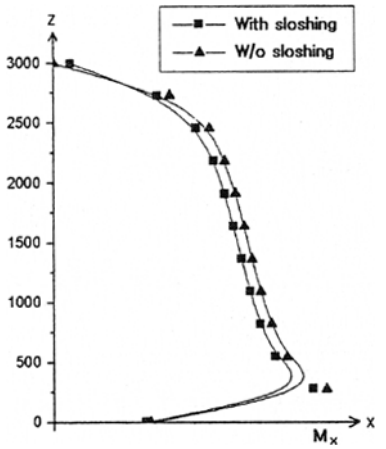

(a) Vertical distributions (m_x at 0°)

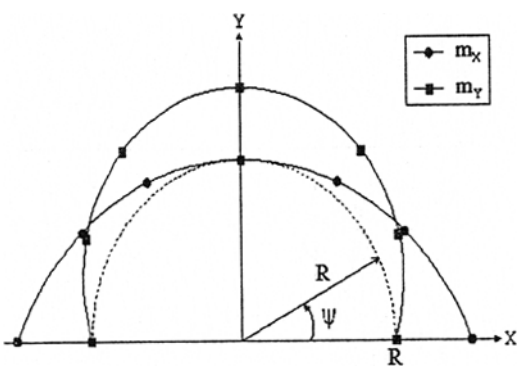

(b) XY-sectional distributions

Fig. 6 Vertical and sectional distributions of the computed nodal masses

tional distribution while the y-component shows sine-type sectional distribution.

With the computed added-mass matrices for both cases with and without the free-surface sloshing (fluctuation), we calculate natural frequencies up to forty natural modes (to retain numerical errors in the considering lowest modes) by the iterative numerical algorithm presented in Fig. 4. In order to examine the effect of the suitability of added mass, we consider two additional mass-adding cases. For the method I, we add the same 61.7% of the total LNG-mass as the classical method such that the added-mass components have cosine- and sine-type distributions shown in Fig. 6(b) along the circumferential direction but the uniform distribution in the

Table 2 The computed lowest natural frequencies (rad/sec) of bulging mode

Mode	Present method		Rough analysis	
	With sloshing	W/o sloshing	Method I	Method II
1st	7.99407	7.82046 (-2.172 %)	9.43351 (18.007 %)	10.53539 (31.790 %)
2nd	12.91134	12.82327 (-0.682 %)	15.76890 (22.132 %)	17.63313 (36.571 %)
3rd	16.47090	16.39349 (-0.470 %)	20.16092 (22.403 %)	22.56515 (37.000 %)
4th	17.84708	17.77147 (-0.424 %)	22.03941 (23.490 %)	24.44500 (36.969 %)

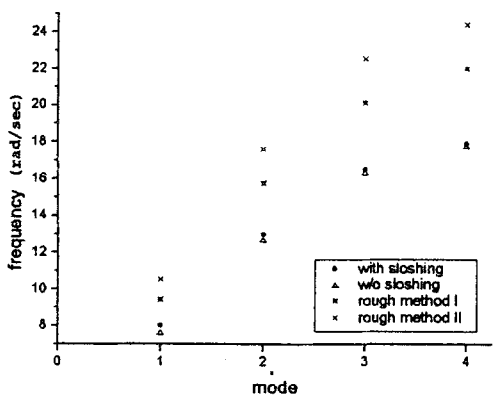

Fig. 7 Comparison of natural frequencies obtained by the four different mass-adding methods

axial direction. While, for the method II, the same amount of LNG-mass but with the uniform distribution along the axial and the circumferential directions is added.

Table 2 contains the computed results of four lowest natural frequencies for the four different mass-adding approaches, where the relative variations are calculated with respect to the case with the liquid free-surface sloshing. Due to the relatively bigger amount in total added mass, the case without sloshing produces relatively lower natural frequencies compared to the case with sloshing. However, the difference between both cases is not considerable and furthermore it monotonically decreases as the natural frequency goes up. On the other hand, the numerical results obtained by the other two approaches are significantly higher compared the values by the present methods, particularly by method II. This is solely owing to the unsuitability of the spatial distribution of added mass. The higher values in natural frequencies are because the added-mass amount unaffecting the bulging mode is involved in the uniform spatial added-mass distributions.

Fig. 8 shows the mode-shapes corresponding to four lowest natural frequencies obtained by the present method with the liquid free-surface sloshing.

4.2 Results of the sloshing mode

With the developed test FEM program according to the theoretical and numerical results described in this paper, we carry out the numerical simulation for the sloshing mode with the uniformly partitioned finite-element mesh. We compute the same number of natural frequencies as the bulging mode, and we compare the numerical results obtained by the rigid-tank and the flexible -tank models.

Table 3 contains the comparative numerical results of four lowest natural frequencies of the both cases. Since the container-deformation becomes smaller as the natural frequency goes lower, as mentioned earlier, the difference in both cases significantly decreases in proportion to the decrease in the natural frequency. For our model problem, the relative difference with respect to the rigid tank is far less than 1%, up to the fourth eigenmode. The mode-shapes corresponding to four lowest natural frequencies of the horizontal sloshing eigen-behavior are depicted in Fig. 9.

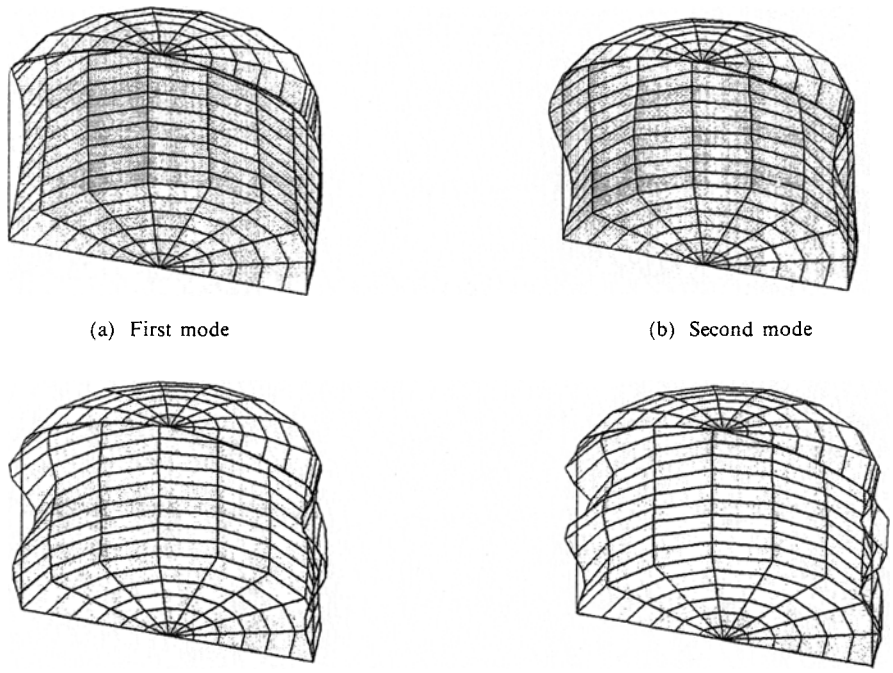

(a) First mode (b) Second mode

(c) Third mode (d) Fourth mode

Fig. 8 Bulging mode shapes of four lowest natural frequencies in the structure motion

Table 3 Computed lowest natural frequencies (rad/sec)

Mode	Rigid tank	Flexible tank	Relative difference
1	0.82727	0.82727	0 %
2	1.38023	1.38023	0 %
3	1.68254	1.68464	0.125 %
4	1.84968	1.85340	0.201 %

As one can infer from the derivation process of Appendix A.2, the effect of container-deformation on the sloshing mode has different degrees of intensity for different material, geometry data and boundary conditions of liquid-storage tank. From the qualitative point of view, the relative contribution of added-mass by the container -deformation is closely proportional to the relative flexibility of the container to the interior liquid.

5. Conclusions

This paper addresses the study on finite element analysis of the horizontal eigen-behavior of LNG -storage tanks equipped with tightening anchor bolts. We first constructed two separate eigen problems for the bulging mode and the sloshing mode, respectively. In order to assure the modeling quality for the LNG-structure hydrodynamic interaction, we particularly took into consideration of the container-deformation in the bulging mode and the LNG free-surface fluctuation in the added-mass computation.

On the other hand, for the numerical experiments we developed a test FEM program according to our theoretical results, in which we introduced an iteration algorithm utilizing the Lanczos technique and the frontal solver for an efficient treatment of inherent large-scale matrices.

According to the refinement of classical simplified models for both eigen modes by including the two neglected effects, we found that both

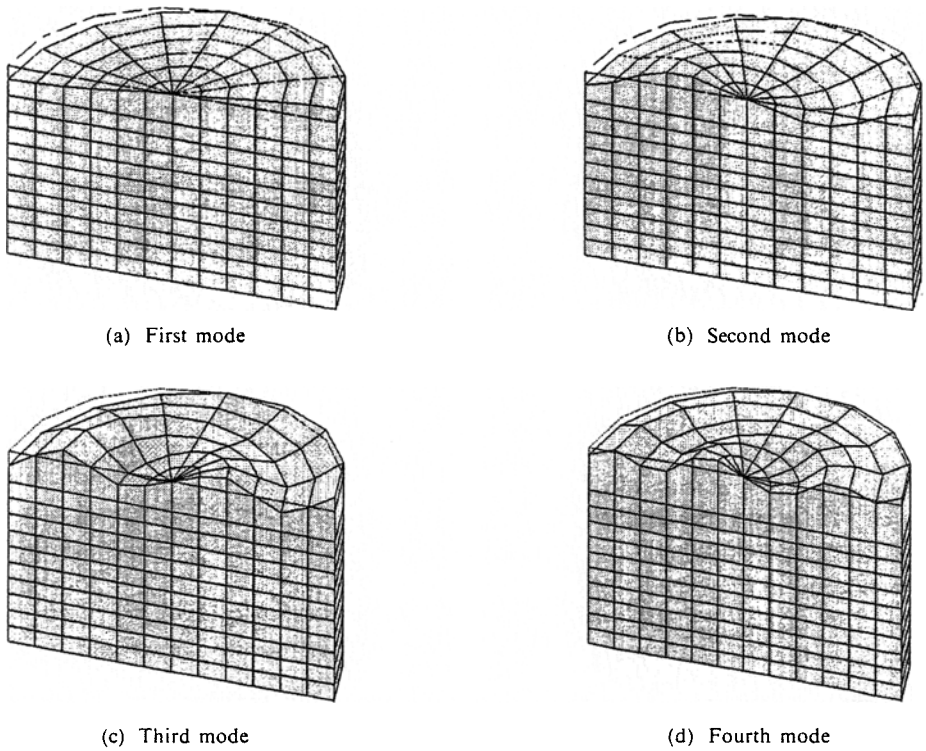

(a) First mode (b) Second mode

(c) Third mode (d) Fourth mode

Fig. 9 Sloshing mode shapes of four lowest natural frequencies in the LNG motion.

bulging and sloshing modes become frequency-dependent eigen problems. In order to compute frequency-dependent eigen frequencies and modes of the sloshing mode, we employed a sort of predictor and corrector numerical technique.

For the bulging mode, we first computed added-mass matrix and analyzed its frequecy-wise variation and spatial distributions for the cases with and without the LNG free-surface fluctuation. We observed that the difference in added masses between both cases is remarkable at the LNG free surface and in lower natural frequency range. And the refined model produced the relatively smaller total added masses and accordingly relatively higher eigen frequencies, when compared to the classical model.

With the four different spatial added-mass distributions, we carried out the comparative numerical experiments. Compared to the present method described in this paper, the two rough methods produced eigen frequencies with considerable error, owing to the inappropriate spatial distribution of added mass, even though the same total amount of mass was added. On the other hand, the effect of LNG free-surface fluctuation on the bulging mode diminished as the natural frequency becomes higher.

From the numerical results of the sloshing mode, we observed that the difference in eigen frequencies between the classical rigid-tank model and the present flexible-tank model prevails in proportion to the decrease of frequency. This frequency variation is reverse to that of the bulging mode, however it is consistent well with the physical interpretation. That is, the container-deformation prevails while the LNG free-surface fluctuation diminishes, as the natural frequency becomes higher.

Acknowledgment

The financial support for this study by *Korea Science and Engineering Foundation* (Grant No. 981-1002-016-2) and *Samsung Heavy Industries* is gratefully acknowledged.

References

Bathe, K. J., 1996, *Finite Element Procedures*, Prentice Hall.

Chen, W., Haroun, M. A. and Liu, F., 1996, "Large Amplitude Liquid Sloshing in Seismically Excited tanks," *Earthquake Engineering and Structural Dynamics*, Vol. 25, pp. 653~669.

Conca, C., Osses, A. and Planchard, J., 1997, "Added Mass and Damping in Fluid-Structure Interaction," *Computer Methods in Applied Mechanics and Engineering*, Vol. 146, pp. 387~405.

Currie, I. G., 1974, *Fundamental Mechanics of Fluids*, McGraw-Hill.

Gupta, K. K., 1976, "On a Numerical Solution of the Supersonic Panel Flutter Eigen Problem," *Int. J. for Numerical Methods in Engineering*, Vol. 10, pp. 637~645.

Haroun, M. A. and Tayel, M. A., 1985, "Axisymmetrical Vibrations of Tanks-Numerical," *J. of Engineering Mechanics*, Vol. 111, No. 3, pp. 329~345.

Haroun, M. A., 1983, "Vibration Studies and Tests of Liquid Storage Tanks," *J. of Earthquake Engineering and Structural*, Vol. 11, pp. 179~206.

Khai, S. L., 1993, "Seismic Coupled Modeling of Axisymmetric Tanks Containing Liquids," *J. of Engineering Mechanics*, Vol. 119, No. 9, pp. 1747~1761.

Kwak, J. Y. and Yoo, H. H., 1998, "Vibration Analysis of a Pretwisted Rotating Blade with a Concentrated Mass," *Transactions. of the KSME (A)*, Vol. 22, No. 1, pp. 190~197.

Morand, H. J.-P. and Ohayon, R., 1995, *Fluid Structure Interaction: Applied Numerical Methods*, Wiley.

Okada, M., Sakai, F. and Sakoda, H., 1975, "Earthquake Response Analysis of Large Tanks Containing Liquid by Finite Element Method," *Kawasaki Technical Report*, Vol. 59, pp. 69~74.

Rajasankar, J., Iyer, N. R. and Apparao, T. V. S. R., 1993, "A New Finite Element Model to Evaluate Added Mass and for Analysis of Fluid-Structure Interaction Problems," *Int. J. for Numerical Method Methods in Engineering*, Vol. 36, pp. 997~1012.

Tedesco, J. W., Landis, D. W. and Kostem, C. N., 1989, "Seismic Analysis of Cylindrical Liquid Storage Tanks," *Computers & Structures*, Vol. 32, No. 5, pp. 1165~1174.

Zienkiewicz, O. C. and Taylor, R. L., 1991, *The Finite Element Method*, 4th Edition, McGraw-Hill.

Appendix

A.1 Equivalent added-mass of LNG

Taking a time derivative to Eq. (18) together with the fundamental relation given in Eq. (14) leads to the alternative system of equations

$$(\mathbf{K}-\omega^2\mathbf{M})\,\bar{\mathbf{p}}=\rho_L\,\mathbf{H}\ddot{\bar{\mathbf{u}}}_n \tag{A1}$$

Denoting $(\mathbf{K}-\omega^2\,\mathbf{M})$ by $\mathbf{S}(\omega)$ and splitting the global finite-element nodes into those (denoted by I) on the liquid-structure interface $\partial\Omega_I$ and the rest (denoted by R), we have

$$\begin{bmatrix}\mathbf{S}_{II} & \mathbf{S}_{IR}\\ \mathbf{S}_{RI} & \mathbf{S}_{RR}\end{bmatrix}\begin{Bmatrix}\bar{\mathbf{p}}_I\\ \bar{\mathbf{p}}_R\end{Bmatrix}=\rho_L\begin{bmatrix}\mathbf{H} & \mathbf{0}\\ \mathbf{0} & \mathbf{0}\end{bmatrix}\begin{Bmatrix}\ddot{\bar{\mathbf{u}}}_n\\ \mathbf{0}\end{Bmatrix} \tag{A2}$$

Applying the static condensation, we obtain the relation at the interface between the hydrodynamic pressure and the normal dynamic acceleration of the structure given by

$$\bar{\mathbf{p}}_I=\rho_L[\mathbf{S}_{II}-\mathbf{S}_{IR}\mathbf{S}_{RR}^{-1}\mathbf{S}_{RI}]^{-1}\mathbf{H}\ddot{\bar{\mathbf{u}}}_n=\rho_L\mathbf{S}_I^{-1}\mathbf{H}\ddot{\bar{\mathbf{u}}}_n \tag{A3}$$

Next, we define the coordinate transformation operator $\mathbf{R}$ which transforms a vector in Cartesian coordinate into the normal component to the structure interface such that

$$\mathbf{R}:\mathbf{u}\in\Re^3\rightarrow u_n\in\Re,\ \mathbf{R}\mathbf{R}^T=\mathbf{I} \tag{A4}$$

Then, the finite element approximation of the second term in the RHS of Eq. (4) indicating the virtual work by the hydrodynamic pressure leads to:

$$\begin{aligned}\int_{\partial\Omega_I}\mathbf{v}_n^h\mathbf{p}_I^h\,ds&=\int_{\partial\Omega_I}[\Phi(\mathbf{R}\bar{\mathbf{v}})]^T[\Phi(\rho_L\mathbf{S}_I^{-1}\mathbf{H}(\mathbf{R}\ddot{\bar{\mathbf{u}}}))]ds\\&=(\mathbf{R}\bar{\mathbf{v}})^T\left\{\int_{\partial\Omega_I}\rho_L\Phi^T\Phi\,ds\right\}[\mathbf{S}_I^{-1}(\mathbf{H}\mathbf{R})\ddot{\bar{\mathbf{u}}}]\\&=\rho_L\bar{\mathbf{v}}^T(\mathbf{R}^T\mathbf{H})\mathbf{S}_I^{-1}(\mathbf{H}\mathbf{R})\ddot{\bar{\mathbf{u}}}\\&=-\omega^2\bar{\mathbf{v}}^T[\rho_L(\mathbf{H}\mathbf{R})^T\mathbf{S}_I^{-1}(\mathbf{H}\mathbf{R})]\bar{\mathbf{u}}\end{aligned} \tag{A5}$$

Here, Φ is the finite-element basis-matrix introduced in Eq. (17) and $\mathbf{H}$ the symmetric matrix defined in Eq. (19), respectively. The term $[\cdot]$ in the last line in above equation is the frequency-dependent added-mass matrix $\mathbf{M}_{add}$ added to the structure.

From the definition of added-mass matrices and the fact of $(p|_{\partial\Omega_F}=\rho_L g\eta)$ by relating Eq. (14) with Eq. (15), the frequency-dependent term $\omega^2\mathbf{M}\bar{\mathbf{p}}$ in Eq. (A1) can be converted to the following expressing the effect of the LNG free-surface sloshing

$$\rho_L g\omega^2\mathbf{M}\bar{\eta} \tag{A6}$$

Therefore, the frequency-dependence of added-mass weakens as the natural frequency becomes higher because the free-surface fluctuation height η significantly diminishes in proportion to the increase of frequency.

A.2 Effect of the structure-deformation

Returning to the variational form (4), we re-write the virtual work done by the hydrodynamic pressure as

$$\int_{\partial\Omega_I} p\mathbf{v}\cdot\mathbf{n}\ ds=\int_{\partial\Omega_I}\mathbf{v}^T\mathbf{p}\ ds \tag{A7}$$

with $\mathbf{p}$ in Cartesian coordinates and we approximate this vector using the basis matrix defined in Eq. (5) such that

$$\mathbf{p}^h=\mathbf{N}\bar{\mathbf{p}} \tag{A8}$$

Then, the finite element approximation of the problem (4) results in

$$[\mathbf{K}-\omega^2\mathbf{M}]\bar{\mathbf{u}}=-\mathbf{G}\bar{\mathbf{p}}_I \tag{A9}$$

with the stiffness matrix $\mathbf{K}$ by the container and anchor bolts and $\mathbf{M}$ indicating the first term in the RHS of Eq. (10) together with $\mathbf{G}$ defined as

$$\mathbf{G}=\int_{\partial\Omega_I}\mathbf{N}^T\mathbf{N}\ ds \tag{A10}$$

By applying the mass-lumping technique and splitting the global finite element nodes over the entire container domain Ω into those (denoted by I) on the liquid-structure interface and the rest (denoted by S), we have

$$\begin{bmatrix}\mathbf{K}_{II}-\omega^2\mathbf{M}_{II} & \mathbf{K}_{IS}\\ \mathbf{K}_{SI} & \mathbf{K}_{SS}-\omega^2\mathbf{M}_{SS}\end{bmatrix}\begin{Bmatrix}\bar{\mathbf{u}}_I\\ \bar{\mathbf{u}}_S\end{Bmatrix}=-\begin{bmatrix}\mathbf{G} & \mathbf{0}\\ \mathbf{0} & \mathbf{0}\end{bmatrix}\begin{Bmatrix}\bar{\mathbf{p}}_I\\ \mathbf{0}\end{Bmatrix} \tag{A11}$$

After the static condensation, we have

$$\begin{aligned}\bar{\mathbf{u}}_I&=-[(\mathbf{K}_{II}-\omega^2\mathbf{M}_{II})\\&\quad-\mathbf{K}_{IS}(\mathbf{K}_{SS}-\omega^2\mathbf{M}_{SS})^{-1}\mathbf{K}_{SI}]^{-1}\mathbf{G}\bar{\mathbf{p}}_I\\&=\mathbf{Q}(\omega)\bar{\mathbf{p}}_I\end{aligned} \tag{A12}$$

Transforming two nodal vectors $\bar{\mathbf{u}}_I$ and $\bar{\mathbf{p}}_I$ expressed in Cartesian coordinates into normal nodal vectors using the operator defined in Eq. (A4), we have together with the relation (14)

$$\bar{\mathbf{u}}_n=-\rho_L\mathbf{R}^T\mathbf{Q}(\omega)\mathbf{R}\bar{\vec{\varphi}}_I \tag{A13}$$

Next, we define a matrix operator (composed of 0 and 1) extending a nodal vector confined within the liquid-structure interface to one containing entire finite-element nodes in the liquid domain such that, for any matrix multiplied to $\bar{\mathbf{u}}|_{\partial\Omega_I}$

$$\mathbf{D}:\mathbf{A}\bar{\mathbf{u}}|_{\partial\Omega_I}\rightarrow\mathbf{A}\mathbf{D}\mathbf{u}|_{\Omega_L} \tag{A14}$$

Taking time derivative to Eq. (A13) together with the extension operator $\mathbf{D}^T$, we obtain

$$\begin{Bmatrix}\hat{\mathbf{u}}_n^F\\ \hat{\mathbf{u}}_n^R\end{Bmatrix}=\rho_L\omega^2(\mathbf{RD})^T\mathbf{Q}(\mathbf{RD})\begin{Bmatrix}\bar{\varphi}_F\\ \bar{\varphi}_R\end{Bmatrix} \tag{A15}$$

Then, it is not hard to arrive at Eq. (20) by substituting Eq. (A15) into Eq. (18).